Journal of Materials Chemistry A

Accepted Manuscript

ROYAL SOCIETY OF CHEMISTRY

www.rsc.org/materialsA

Cite this: DOI: 10.1039/c0xx00000x

www.rsc.org/xxxxxx

ARTICLE TYPE

Aqueous- and vapor-phase detection of nitroaromatic explosives by a water-stable fluorescent microporous MOF directed by ionic liquid

Jianhua Qin,[a,b] Bing Ma,[a] Xiao-Fei Liu,[a] Hong-Lin Lu,[a] Xi-Yan Dong,[a] Shuang-Quan Zang*[a] and Hongwei Hou*[a]

Received (in XXX, XXX) Xth XXXXXXXXX 20XX, Accepted Xth XXXXXXXXX 20XX
DOI: 10.1039/b000000x

A water-stable fluorescent microporous metal-organic framework (MOF), [Tb(L)(OH)] ·x(solv) (**1**), has been designed and successfully synthesized under the combination of hydro/solvothermal and ionothermal condition (H_2L = 5-(4-carboxyphenyl)pyridine-2-carboxylate). The crystal structure reveals that complex **1** consists of cubane-shaped tetranuclear terbium building units, which are further bridged by the multicarboxylate ligands to give a (3,12)-connected topology with the point symbol $(4^{20}.6^{28}.8^{18})(4^3)_4$. More importantly, excellent hydrolytic stability allows it to be used in an aquatic system, which is highly desirable for practical applications. Activated **1** shows high selectivity and sensitivity towards nitroaromatic explosives in both aqueous and vapor phase. The sizes of the pore windows (11.2 × 11.2 Å^2) in **1**, which are larger than the size of the selected nitroaromatics, could permit easy diffusion of analytes inside the channel, keeping the electron rich framework and electron deficient analytes in close proximity.

Introduction

Selective and sensitive detection of highly explosive and explosivelike substances has become a serious issue concerning homeland security, environmental monitoring, military applications, forensic investigations, and mine-field analysis.[1,2] Nitroaromatic explosives such as 2,4,6-trinitrotoluene (TNT), 2,4-dinitrotoluene (2,4-DNT), 2,4,6-trinitrophenol (TNP), and nitrobenzene (NB) are common ingredients of industrial explosives and found in many unexploded land mines worldwide.[1f] Current high-explosive detection methods typically involve canines or sophisticated instruments like gas chromatography coupled with mass spectrometry,[3] surface enhanced Raman spectroscopy,[4] cyclic voltammetry[5] and ion mobility spectrometry (IMS),[1c] which are not very efficient for explosives detection in the field because of limited portability, high cost and great complexity.[2d,2f] Recently, fluorescence-based detection methods based on the electron transfer and/or energy transfer mechanisms, have attracted increasing attention due to their high sensitivities, portability, low cost, short response times, and dual compatibility in solid and solution media.[1,2] A large number of fluorescent materials including conjugated polymers,[1,6] nanoparticles[1b-1f,7,8] and microporous metal-organic frameworks (MMOFs)[2,9,10] have been employed for explosive detection. The combination of fluorescence and accessible porosity within MMOFs imparts them with the capability of transducing the host–guest chemistry to detectable changes in fluorescence and makes them promising candidates for sensing applications. Moreover, for in-field selective detection of nitroaromatic explosives present in soil and ground water, probe working in aqueous media is highly desirable. Although MMOFs have been employed for liquid phase nitroaromatic explosive detection, to the best of our knowledge, the precedence of MMOFs as an explosive sensor in the desired aqueous medium is indeed rare.[11] Additionally, vapor phase detection of nitroaromatic explosives by fluorescence quenching methods employing the thin film of MMOFs has been proven to be very effective.[10]

Ionic liquids (ILs), a class of salts which are liquid at low temperature and consist of ions only, have received increasing attention as the solvent of choice for the syntheses of crystalline materials such as zeolites and MOFs.[12-15] Recently, Su group and our group demonstrated the combination of hydro/solvothermal and ionothermal methods.[16] Herein we report the fluorescent property and sensing behavior of [Tb(L)(OH)] ·x(solv) (**1**) (H_2L = 5-(4-carboxyphenyl)pyridine-2-carboxylate; solv = H_2O, N, N-Dimethylformamide (DMF)) directed by [BMI]Br IL (BMI = 1-butyl-3-methylimidazolium). H_2L was chosen to build fluorescent MMOFs targeted for sensing applications because its highly conjugated π-systems could act as both the sources of fluorescence and the chemical recognition elements (binding sites). In addition to helping solubilise the starting materials under the reaction conditions there is evidence that [BMI]Br itself can play a structure directing role and is intimately involved in template ordering in [Tb(L)(OH)], even though neither $[BMI]^+$ cation nor Br^- anion is occluded into the ultimate structure. We envisioned that the sizes of the pore windows (11.2 × 11.2 Å^2) in **1**, which are larger than the size of the selected nitroaromatics, could permit easy diffusion of analytes inside the channel, keeping the electron rich MMOF and electron deficient analytes in close proximity. More importantly, excellent hydrolytic

stability allows it to be used in an aquatic system, which is highly desirable for practical applications. As expected, the fluorescence of activated **1** (referred to as **1'** hereafter) shows high selectivity and sensitivity towards the presence of trace amount of nitroaromatic analytes in both aqueous and vapor phase, which shows its potential as explosive sensor. Our study suggests that the nature of the analyte molecules, the electronic structure and porosity of the MMOF all play key roles in the observed fluorescence quenching behaviors.

Experimental section

Materials and physical measurements

All chemicals were of reagent grade quality, and they were purchased from commercial sources and used as received. Elemental analysis for C and H were performed on a Perkin-Elmer 240 elemental analyzer. The FT-IR spectra were recorded from KBr pellets in the range from 4000 to 400 cm^{-1} on a Bruker VECTOR 22 spectrometer. Thermal analyses were performed on a SDT 2960 thermal analyzer from room temperature to 800 ℃ at a heating rate of 20 ℃/min under nitrogen flow. Powder Xray diffraction (PXRD) data were collected on a Rigaku D/Max-2500PC diffractometer with Cu Kα radiation (λ = 1.5406 Å) over the 2θ range of 5−50 ° with a scan speed of 5 °/min at room temperature. Fluorescence spectra were recorded on a Hitachi 850 fluorescence spectrophotometer.

Synthesis of [Tb(L)(OH)] ₓ(solv)

First step: $Tb(NO_3)_3$ $6H_2O$ (0.20 mmol) and H_2L (0.10 mmol) were soaked in 1 mL [BMI]Br solution (BMI = 1-butyl-3-methylimidazolium) in a glass vial (10 mL), which was heated in an isotherm oven more than 100 ℃ until starting materials dissolved.

Second step: 4 mL mixed solvent of N, N-Dimethylformamide (DMF) and H_2O (V/V = 1:1) was added, and then the homogeneous phase was transferred to a 25 mL Teflon-lined stainless steel vessel. The vessel was sealed and heated to 160 ℃ for 72 h and then cooled to room temperature at a rate of 5 ℃ h^{-1}. Colorless crystals of **1** were obtained with a yield of 89% (based on H_2L). IR (cm^{-1}, KBr): 3430 bv, 1642 s, 1541 s, 1384 s, 1170 m, 1010 w, 813 w, 785 m, 681 m.

Note that **1** could only be obtained in the presence of [BMI]Br. Many tries to synthesize the complex under traditional hydro/solvothermal conditions failed.

X-ray crystallography

Single crystal X-ray diffraction analysis of **1** was carried out on a Bruker SMART APEX CCD diffractometer[17] using graphite-monochromatized Mo Kα radiation (λ = 0.71073 Å) at room temperature using the ω-scan technique. The structures were solved by direct methods with SHELXS-97[18] and refined by the full-matrix least-squares method on F^2 with anisotropic thermal parameters for all non-H atoms (SHELXL-97)[19]. The empirical absorption corrections were applied by the SADABS program.[20] The hydrogen atoms were assigned with common isotropic displacement factors and included in the final refinement by use of geometrical restrains. There is large solvent accessible void volume in **1** which is occupied by highly disordered free solvent molecules. No satisfactory disorder model could be achieved, and therefore the SQUEEZE program implemented in PLATON was used to remove its electron densities.[21] The crystallographic data and selected bond lengths and angles for **1** are listed in Tables S1 and S2 in ESI†. Crystallographic data for the structural analysis have been deposited with the Cambridge Crystallographic Data Center. CCDC number for **1** is 1042544.

Experiments of detecting of nitroaromatic explosives in the aqueous phase

The fine grinding sample **1'** (2 mg) was dispersed in 1 mM or saturated aqueous solutions (2 mL) of a series of nitroaromatics, treated by ultrasonication for 30 min and then aged for 3 days to form a stable emulsion before the fluorescence studies. The nitroaromatics used in this study were nitrobenzene (NB), 2-nitrotoluene (2-NT), 1,3-dintrobenzene (1,3-DNB), 1,4-dintrobenzene (1,4-DNB), 2,4-dinitrotoluene (2,4-DNT), 2,6-dinitrotoluene (2,6-DNT), 2,4,6-trinitrotoluene (TNT), 2,4,6-trinitrophenol (TNP). As a comparison, the emission spectra and fluorescent intensity for **1'** dispersed in methyl cyanide (MeCN), and N,N-dimethylformamide (DMF), and even other aromatic compounds, such as benzene (BZ), toluene (TO), bromobenzene (BrBZ), *p*-xylene (PX), were also recorded. In fluorescence titration setup, 2 mg of **1'** was dispersed in 2 mL aqueous solution, treated by ultrasonication for 30 min and then aged for 3 days for the next experiment. The fluorescence was measured in-situ after incremental addition of freshly prepared 1 mM or saturated aqueous solutions of each analyte. All the experiments were performed in triplicate and consistent results are reported. The quenching efficiency (%) was estimated using the formula $(F_0 - F)/F_0 \times 100\%$, where F_0 and F are the maximum fluorescent intensity of **1'** before and after the addition of analyte, respectively.

Experiments of detecting of nitroaromatic explosives in the vapor phase

The real-time solid–gas detection of the selected analytes vapor was implemented by using the sample of **1'** as the starting material. Finely ground powder sample of **1'** (3 mg) was loaded on a quartz plate. Absolute ethanol (0.5 mL) was then added to the sample to afford a slurry. The quartz plate was then standing to produce a coating on the plate (while the ethanol was evaporative). The ethanol completely evaporated after about 3 minutes. This coating device was placed into a sealed optical quartz cuvette, wherein 10 mg (1,3-DNB, 1,4-DNB, 2,4-DNT, 2,6-DNT, TNT, TNP) or 1 ml (NB, 2-NT) was also seated, respectively. After specified exposure time, the emission spectrum was recorded. The quenching efficiency (%) was estimated using the formula $(F_0 - F)/F_0 \times 100\%$, where F_0 and F are the maximum fluorescent intensity of **1'** before and after exposure to analyte vapor, respectively.

Results and discussion

Structure description of [Tb(L)(OH)]

Single crystal X-ray analysis indicated that **1** crystallizes in tetragonal crystal system *I*4(1)/*a* space group and features a noninterpenetrated open three-dimensional (3D) porous framework constructed by infinite unique cubane-shaped $[Tb_4(\mu_3\text{-}OH)_4]^{8+}$ tetranuclear-based[22], rod-shaped lanthanide-carboxylate

SBUs and L linkers. The asymmetry unit of **1** is composed of one crystallographically unique eight-coordinated Tb(III) ion, one L ligand and one μ_3-hydroxyl group (Fig. 1a). Overall each central Tb(III) ion coordinates to four oxygen and one nitrogen atoms from four different L ligands as well as three μ_3-hydroxyl oxygen atoms. The Tb–N bond length is 2.577(5) Å, whereas the Tb–O bond lengths vary from 2.347(4) to 2.431(4) Å. Four triply bridging μ_3-hydroxyl oxygen atoms link four Tb(III) ions to form a cubane-shaped tetranuclear $[Tb_4(\mu_3\text{-}OH)_4]^{8+}$ cluster (Fig. S1 in ESI†), which is surrounded by twelve L ligands and connected into 1D rod-shaped Tb(III)-carboxylate chains by carboxylate groups (Fig. 1b). The two carboxylate groups in a separate L ligand are deprotonated and adopt κ^5 $N,O^2:O^{2'}:O^4:O^{4'}$-μ_4 bridging mode (Fig. S2 in ESI†) to link the Tb(III) ions, resulting in the formation of a 3D porous framework (11.2 × 11.2 $Å^2$) with a void volume of 3145.5 $Å^3$ per unit cell, which is 41.4% of the total crystal volume after removal of the various solvents from the pores (calculated by PLATON) (Fig. 1c and Fig. S3 in ESI†). Furthermore, topological analysis is carried out to get insight of the structure of **1**. If $[Tb_4(\mu_3\text{-}OH)_4]^{8+}$ cluster is considered as a twelve-connected node which is linked with twelve L ligands, and L ligand is regarded as a three-connected node, as shown in Fig. 1d and Fig. S4-S5 in ESI†, the structure can be viewed as a (3,12)-connected topology with the point symbol $(4^{20}.6^{28}.8^{18})(4^3)_4$.

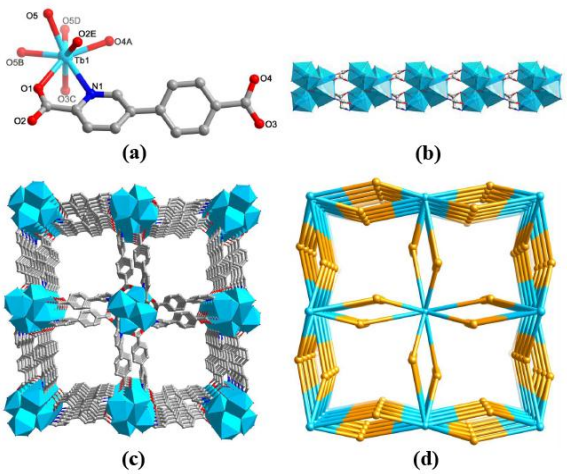

Fig. 1 (a) The coordination environment of Tb(III) ion. Symmetry codes (A) -x, -y+2, -z; (B) -x, -y+3/2, z; (C) -y+5/4, x+3/4, z-1/4; (D) y-3/4, -x+3/4, -z-1/4; (E) -y+3/4, x+3/4, -z+3/4. (b) The rod-shaped Tb(III)-carboxylate SBU. (c) Ball and stick representation of the channels along the *c*-axis direction. (d) Schematic representation of the (3,12)-connected $(4^{20}.6^{28}.8^{18})(4^3)_4$ topology.

Thermal and water stability

Considering practical applications, the robustness and water stability of the compound were firstly investigated. Thermogravimetric analysis (TGA) indicated framework of **1** has excellent stability. The TGA curve of **1** displays a gradual weight loss of about 30% up to 450 ℃, corresponding to the loss of water and DMF molecules (Fig. S6 in ESI†). The guest water and DMF molecules incorporated in **1** can be removed by solvent exchange with CH_2Cl_2 followed by pumping under vacuum at 40 ℃, and the guest-free **1** was verified by TGA on the activated sample. **1'** displayed similar thermal stability to the as-synthesized sample. The PXRD pattern of **1'** confirms the stability of the host framework upon solvent removal. When **1'** was soaked in water for several weeks, retention of crystallinity was observed, as was evidenced by PXRD analysis (Fig. 2), affirming the hydrolytic stability. Furthermore, to confirm the stability of **1'** in aqueous solutions of the selected analytes, we measured the PXRD spectra of the immersed samples (Fig. 2). The recorded patterns gave the same diffraction peaks as those of as-synthesized samples and the simulated patterns from single crystal structure, which proves that its framework is retained in the suspensions.

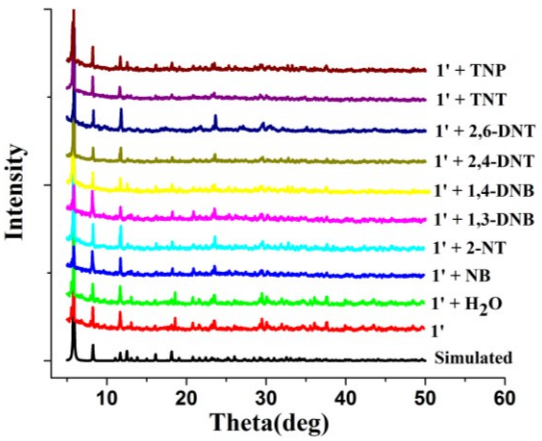

Fig. 2 Powder X-ray diffraction pattern of **1'** obtained after immersing in 1 mM or saturated aqueous solutions of the selected analytes for three days.

Fluorescent properties

The solid state fluorescence behavior of **1'** was recorded at room temperature. The photoluminescence (PL) spectra of **1'** excited at 350 nm are shown in Fig. S7 in ESI†. The fluorescence peaks at 485, 541, 580, and 621 nm could be attributed to the $^5D_4 \rightarrow {}^7F_J$ (J = 3–6) transitions of the Tb^{3+} ions. The dominant band of these emissions is attributed to the hypersensitive transition $^5D_4 \rightarrow {}^7F_5$ of Tb^{3+} ions. We also examined the fluorescent properties of **1'** dispersed in water and common organic solvent. As shown in Fig. S8 in ESI†, **1'** show the strongest emissions in H_2O, MeCN, and DMF, respectively, and the fluorescence peaks at 486, 542, 581, and 620 nm are close to those of solid state sample. The strong emission and stability of **1'** in H_2O suspension indicate its potential to be utilized as a nitroaromatic explosives sensor in the aqueous phase.

Detection of nitroaromatic explosives in the aqueous phase

In actuality, the detection of nitroaromatics in an aquatic system is highly desirable for practical applications.[11] Benefiting from the stability issue in water, the ability of **1'** to sense trace amounts of nitroaromatics in aqueous medium was investigated. The fine grinding sample **1'** was dispersed in 1 mM or saturated aqueous solutions of a series of nitroaromatics. As depicted in Fig. 3, Fig. 4, and Fig. S8 in ESI†, the significant quenching of

fluorescent intensity was observed upon addition of all the selected analytes and above 70% of quenching efficiency could be obtained. Among them, NB, TNP, 2-NT, and TNT could thoroughly quench the emission (quenching efficiency > 99%). In contrast, the emission spectra and fluorescent intensity for **1'** dispersed in MeCN, DMF, and even other aromatic compounds, such as BZ, TO, BrBZ, PX, were recorded and compared. As shown in Fig. S8 in ESI†, all of these organic solvents display a negligible effect on the emission of **1'**. Such observations demonstrate that **1'** has a selective fluorescence response to nitroaromatics compared to other non-nitroaromatics.

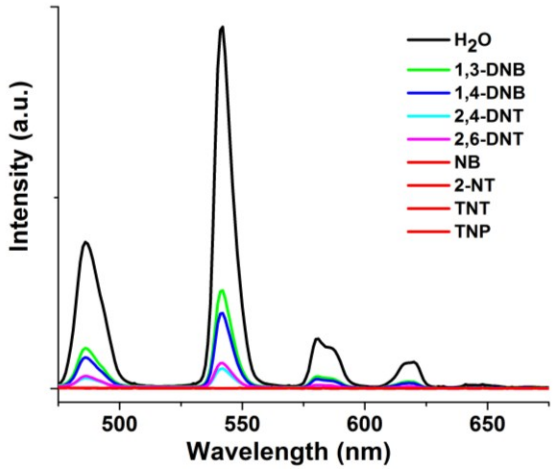

Fig. 3 The emission spectra for **1'** dispersed in H_2O and 1 mM or saturated aqueous solutions of the selected analytes at room temperature.

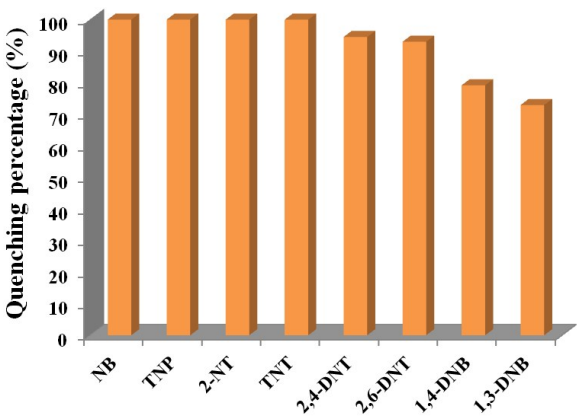

Fig. 4 Quenching efficiency of the fluorescent intensity for **1'** dispersed in 1 mM or saturated aqueous solutions of the selected analytes at room temperature. (excited and monitored at 350 nm and 542 nm, respectively).

To examine sensing sensitivity towards nitroaromatics in more detail, a batch of suspensions of **1'** with gradually increasing the analytes contents in aquatic system was prepared to monitor the emissive response (Fig. 5 and Fig. S9-S14 in ESI†). In all the sensing experiments, the fluorescence quenching efficiency increased drastically with the analytes amount even in the low concentration range and leveled off at high concentration to reach nearly complete quenching (Fig. S15 in ESI†). The quenching efficiency can be quantitatively explained by the Stern–Volmer equation: $(F_0/F)=K_{sv}[Q]+1$, where F_0 and F are the fluorescent intensities before and after addition of the analyte, respectively, K_{sv} is the quenching constant (ppm^{-1}), $[Q]$ is the concentration of the analyte. The SV plot for NB, 2-NT, TNT, and TNP were nearly linear at low concentrations (≦ 120 ppm), and subsequently deviated from linearity, bending upwards at higher concentrations (Fig. S9-S12 in ESI†). The curvature of SV plot may be ascribed to mixed static and dynamics photoinduced electron transfer.[23] The calculated K_{sv} values for NB, 2-NT, TNT, and TNP were 5.02×10^{-2}, 1.30×10^{-1}, 2.47×10^{-2}, and 7.73×10^{-2} ppm^{-1}, respectively, which lie in the normal range for the known MOFs.[24] To the best of our knowledge, such highly selective detection of nitroaromatics in the aqueous phase based on a fluorescent MOF has not been reported so far.[11]

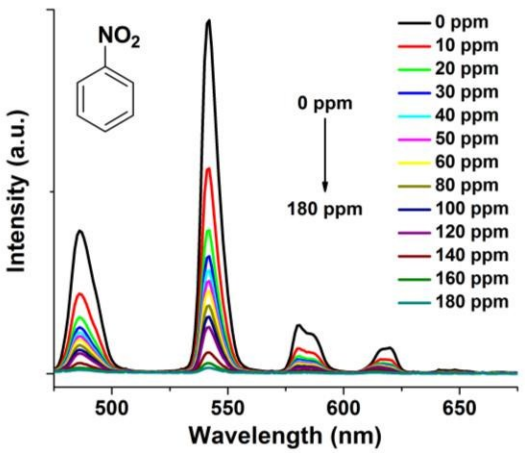

Fig. 5 Fluorescence titration of **1'** dispersed in aqueous solution by gradual addition of NB.

Detection of nitroaromatic explosives in the vapor phase

The vapor pressures of the selected analytes are usually very low at room temperature (Table S3 in ESI†). The real-time solid–gas detection was implemented by using a thin film device placed in a home-made setup. The fluorescence spectra of thin films of **1'** were monitored, before and after exposing them to the equilibrated vapors of different analytes. The fluorescence spectra were recorded immediately after the exposure to analytes vapors. Fig. 6 shows the percentage of fluorescence quenching upon exposure to each analyte vapor after specified time at room temperature. We found that NB, 2-NT, 1,3-DNB, 1,4-DNB, and TNP could act as fluorescence quenchers for **1'**. Among them, the most effective quenchers are NB and 2-NT based on the quenching efficiency, and NB and 2-NT quench the emission by 95% and 86%, respectively. The order of quenching efficiency for the selected analytes is NB > 2-NT > 1,3-DNB > 1,4-DNB > TNP. Notably, this order is not fully in accordance with the trend of electron-withdrawing groups, but it is fully consistent when the vapor pressure of each analyte is also taken into consideration.[10a,10b] The fact that NB and 2-NT exhibit the strongest quenching effect can be attributed to their high vapor

pressure as well as high electron-withdrawing ability. Although vapor pressures of 2,4-DNT and 2,6-DNT are comparable to that of 1,3-DNB and 1,4-DNB, they show no any quenching effect probably due to the presence of the electron-donating -CH_3 group. Similarly, the lower vapor pressure and the more poor electron-withdrawing ability of TNT may account for the zero quenching efficiency to **1'**. Exceptionally, TNP has the lowest vapor pressure and the most poor electron-withdrawing ability, but show a 6% of quenching efficiency (discussed below).

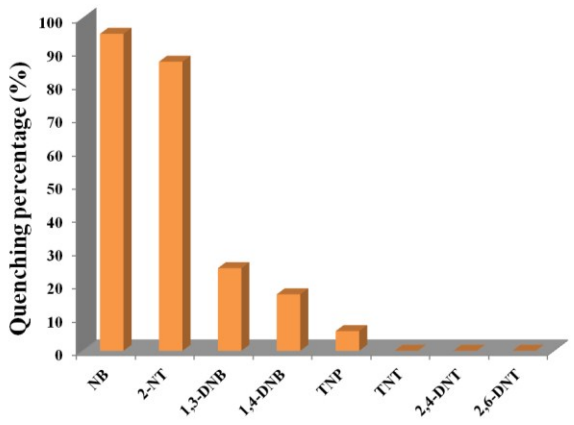

Fig. 6 The percentage of fluorescence quenching upon exposure to each analyte vapor after specified exposure time at room temperature. (excited and monitored at 350 nm and 542 nm, respectively).

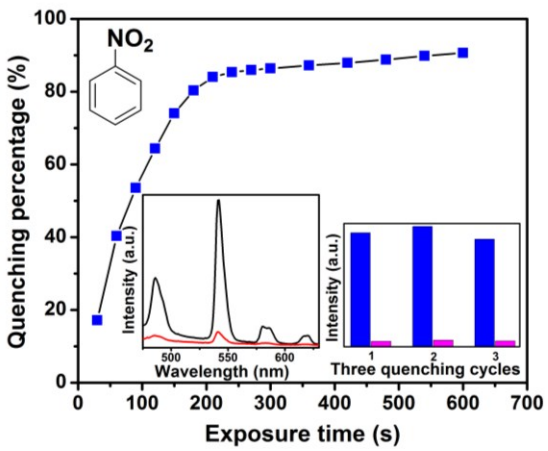

Fig. 7 The time-dependent fluorescence quenching upon exposure to NB vapor. Insets: (left) corresponding emission spectra before and after exposure of **1'** to the NB vapor for ten minutes; (right) results for three continuous quenching cycles.

Furthermore, we have monitored the time-dependent fluorescence quenching profile for each analyte and also compared their relative quenching abilities (Fig. 7 and Fig. S16-S23 in ESI†). **1'** showed almost identically rapid and evident responses to NB and 2-NT, indicating this is a diffusion-controlled fluorescence quenching response. Within ten minutes, the fluorescence quenching percentages reached almost the maxima for both NB and 2-NT (ca. 90% and 80%, respectively). The quenching percentages appeared to approach a constant level given enough exposure time. In addition, detections of both NB and 2-NT with **1'** are fully reversible. After quenching, the fluorescence of **1'** can be recovered by simply heating the thin films at 150 ℃ for about thirty minutes (Fig. 7 and Fig. S16 in ESI†).

Mechanism for the nitroaromatic explosives detecting

The origin of the highly selective sensing nitroaromatic explosives can be attributed to a photoinduced electron transfer from **1'** to the analytes.[2] Although all MOFs have extended network structures, they are often characterized by narrow energy bands because of highly localized electronic states. Therefore, they can be regarded as giant "molecules" and the valence-band (VB) and conduction-band (CB) energy levels can be described in a fashion similar to that used for molecular orbitals (MOs).[10b] In general, the lowest unoccupied MOs (LUMOs) of nitroaromatics are low-lying π*-type orbitals stabilized by the NO_2 group through conjugation,[10b,24d] and their energy is below the CB of **1'**. This can force electrons to transfer from the CB of **1'** to the LUMO of nitroaromatics, thus leading to fluorescence quenching upon excitation. Fig. 8 shows the HOMO and LUMO orbital energies of H_2L and nitroaromatic explosives, as calculated by density functional theory at the B3LYP/6-31G** level (Table S5 in ESI†). As discussed above, the photoluminescence of **1'** is ligand-centered. The electron rich property of the H_2L ligand, which gives a high LUMO energy (-2.30916 eV, higher than the -2.32～-3.90 eV LUMO energy for the tested nitroaromatics) and facilitates the excited state electron transfer from the framework of **1'** to the analyte molecules, is expected to be responsible for the selective response to nitroaromatics.

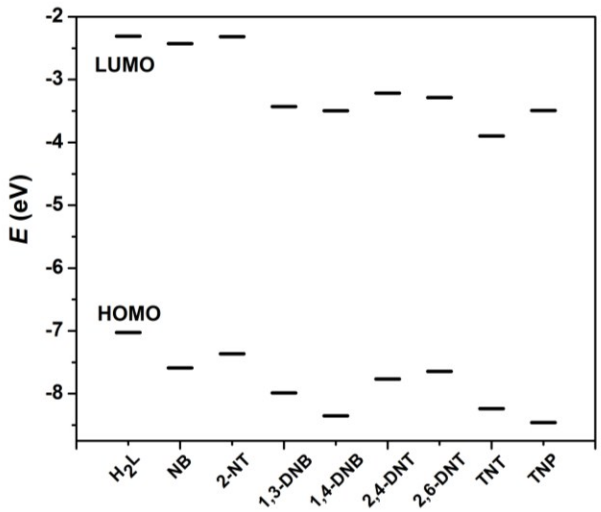

Fig. 8 HOMO and LUMO energies for the selected analytes and the H_2L ligand.

The outstanding sensing capability of **1'** in aqueous and vapor phases, can be further attributed to its infinite 3D framework structure and inherent microporosity.[2d,2f,10a] Related studies about conjugated polymers have pointed out that higher dimensionality enhances sensitivity because the excitons can be quenched by

greater numbers of analyte binding sites through delocalization over the conjugated polymer backbone ("molecular wire" effect).[2d,2f] Analogously, the extended three-dimensional network structure of **1'**, containing ordered π moieties, may also facilitate the migration of the excitons through similar mechanisms. The large optical band gap (ca. 2.7 eV) indicates that the framework in the excited state is highly reductive,[10a] providing an adequate driving force for the electron transfer to analytes (Fig. S24 in ESI†). Since charge transfer was generally considered to be a short range interaction, the channel structures of **1'** should play a significant role in the sensing process. Porous structure has been proven to be a favorable feature for the fast detection of nitroaromatics.[10] The readily accessible micropores in **1'** and the fully exposed internal surface provide facile diffusion routes and binding sites within the ordered framework which can enhance the host–guest interaction by many folds,[2d,2f] accounting for the high sensing sensitivity towards nitroaromatics in both aqueous and vapor phase.

However, the correlation between the quenching efficiency and corresponding LUMO energy of TNP, especially in the vapor phase (the lowest vapor pressure), suggests that the photoinduced electron transfer is not the only mechanism and the long-range energy transfer may also play a key role in such processes.[11,25] The fluorescence of **1'** results from the antenna effect in which the L moieties adsorb the energy and by vibronic coupling between L and Tb^{3+}, transfer energy to Tb^{3+}, leading to the fluorescence of Tb^{3+}. The observed fluorescence attenuation of **1'** upon exposure to TNP vapor is attributed to a competition of absorption of the light source energy between TNP and L moieties.[8a] The TNP filter the light adsorbed by L moieties, thus decreasing the probability of energy transfer from L to Tb^{3+} and subsequently quenching the fluorescence of Tb^{3+}. Related research has shown that the incorporation of different substituents on the aromatic moieties of the nitroaromatic explosives can cause a different degree of red shift of the π to π* transitions of benzene (B band) in the UV-Vis absorption spectrum,[8a] particularly for TNP, which extends the B band to the wavelength beyond 350 nm (Fig. S25 in ESI†).[11] As the excitation wavelength is 350 nm, TNP with higher absorbance and thus higher Ɛ (molar extinction efficient) at 350 nm which suggest the absorption spectrum of TNP has a overlap with the emission spectrum of **1'**, is expected to exhibit stronger quenching effect on the fluorescent intensity of **1'** via energy transfer process.[8a,11] Additionally, the confinement of TNP in the channel structures of **1'** keeps the framework and TNP in close proximity, improving the energy transfer process. Thus it is clear that TNP can efficiently quench the fluorescence of **1'** via both electron and long-range energy transfer processes, which is in contrast to other nitroaromatics which quench fluorescence by an electron transfer process only.

Conclusion

In summary, a highly fluorescent MMOF $[Tb(L)(OH)]\ x(solv)$, has been designed and successfully synthesized based on a highly conjugated π-system ligand as an antenna to sensitize Tb^{3+} emission under the combination of hydro/solvothermal and ionothermal condition. [BMI]Br IL could not only help solubilise the starting materials, but also could be intimately involved in template ordering in **1**. The excellent hydrolytic stability allows **1'** to be used in an aquatic system, which is highly desirable for practical applications. The fluorescence of **1'** shows high sensitivity and sensitivity towards the presence of trace amount of nitroaromatic analytes in both aqueous and vapor phase, probably through a redox quenching mechanism similar to that in the conjugated polymer systems. The origin of the highly selective sensing nitroaromatic explosives can be attributed to a photoinduced electron transfer from **1'** to nitroaromatic explosives. Further analysis demonstrates that TNP can efficiently quench the fluorescence of **1'** via both electron and long range energy transfer processes, while other nitroaromatic explosives quench fluorescence by an electron transfer process only. Clearly, the nature of the analyte molecules and the electronic structure and porosity of the MMOF all play key roles in the observed fluorescence quenching behavior.

Acknowledgments

This work was supported by the National Natural Science Foundation of China (No. 91022013, 21371155 and 21371153) and Program for Science & Technology Innovation Talents in Universities of Henan Province (13HASTIT008) and Key Scientific and Technological Project of Henan Province (132102210411) and Research Found for the Doctoral Program of Higher Education of China (20124101110002).

Notes and references

[a] *College of Chemistry and Molecular Engineering, Zhengzhou University, Zhengzhou 450001, China. E-mail: zangsqzg@zzu.edu.cn; houhongw@zzu.edu.cn.*
[b] *College of Chemistry and Chemical Engineering, Luoyang Normal University, Luoyang 471022, China.*

† Electronic Supplementary Information (ESI) available: [Crystal sturcture, TG plot, photoluminescence spectra, Details of detecting of the analytes, diffuse reflectance spectra, Crystal data, Selected bond lengths and angles, Saturated Vapor Pressure for the analytes, Approximate sizes of the analytes, HOMO and LUMO energies calculated for H_2L and the analytes.]. See DOI: 10.1039/b000000x/

1 (*a*) D. T. McQuade, A. E. Pullen and T. M. Swager, *Chem. Rev.*, 2000, **100**, 2537; (*b*) D. S. Moore, *Rev. Sci. Instrum.*, 2004, **75**, 2499; (*c*) S. J. Toal and W. C. Trogler, *J. Mater. Chem.*, 2006, **16**, 2871; (*d*) S. W. Thomas, G. D. Joly and T. M. Swager, *Chem. Rev.*, 2007, **107**, 1339; (*e*) L. Senesac and T. G. Thundat, *Mater. Today*, 2008, **11**, 28; (*f*) M. E. Germain and M. J. Knapp, *Chem. Soc. Rev.*, 2009, **38**, 2543; (*g*) Y. Salinas, R. Martinez-Manez, M. D. Marcos, F. Sancenon, A. M. Costero, M. Parra and S. Gil, *Chem. Soc. Rev.*, 2012, **41**, 1261.
2 (*a*) Y. Cui, Y. Yue, G. Qian and B. Chen, *Chem. Rev.*, 2012, **112**, 1126; (*b*) L. E. Kreno, K. Leong, O. K. Farha, M. Allendorf, R. P. Van Duyne and J. T. Hupp, *Chem. Rev.*, 2012, **112**, 1105; (*c*) B. Liu, *J. Mater. Chem.*, 2012, **22**, 10094; (*d*) D. Banerjee, Z. Hu and J. Li, *Dalton Trans.*, 2014, **43**, 10668; (*e*) Y. Cui, B. Chen and G. Qian, *Coord. Chem. Rev.*, 2014, **273-274**, 76; (*f*) Z. Hu, B. J. Deibert and J. Li, *Chem. Soc. Rev.*, 2014, **43**, 5815.
3 K. Hakansson, R. V. Coorey, R. A. Zubarev, V. L. Talrose and P. Hakansson, *J. Mass Spectrom.*, 2000, **35**, 337.
4 J. M. Sylvia, J. A. Janni, J. D. Klein and K. M. Spencer, *Anal. Chem.*, 2000, **72**, 5834.
5 M. Krausa and K. Schorb, *J. Electroanal. Chem.*, 1999, **461**, 10.
6 (*a*) A. Rose, Z. Zhu, C. F. Madigan, T. M. Swager and V. Bulovic, *Nature*, 2005, **434**, 876; (*b*) S. J. Toal, D. Magde and W. C. Trogler, *Chem. Commun.*, 2005, 5465; (*c*) J. Lin, C. E. Kending and E. E. Nesterov, *J. Am. Chem. Soc.*, 2007, **129**, 15911; (*d*) J. C. Sanchez and W. C. Trogler, *J. Mater. Chem.*, 2008, **18**, 3143; (*e*) Y. Long, H. Chen,

Y. Yang, H. Wang, Y. Yang, N. Li, K. LI, J. Pei and F. Liu, *Macromolecules*, 2009, **42**, 6501; (*f*) S. Shanmugaraju, S. A. Joshi and P. S. Mukherjee, *J. Mater. Chem.*, 2011, **21**, 9130.

7 (*a*) D. Gao, Z. Wang, B. Liu, L. Ni, M. Wu and Z. Zhang, *Anal. Chem.*, 2008, **80**, 8545; (*b*) Y. Jiang, H. Zhao, N. Zhu, Y. Lin, P. Yu and L. Mao, *Angew. Chem., Int. Ed.*, 2008, **47**, 8601; (*c*) J. Geng, P. Liu, B. Liu, G. Guan, Z. Zhang and M. Y. Han, *Chem.–Eur. J.*, 2010, **16**, 3720; (*d*) J. Feng, Y. Li and M. Yang, *Sens. Actuators*, B, 2010, **145**, 438;

8 (*a*) H. Xu, F. Liu, Y. Cui, B. Chen and G. Qian, *Chem. Commun.*, 2011, **47**, 3153; (*b*) Y. Yuan, W. Wang, L. Qiu, F. Peng, X. Jiang, A. Xie, Y. Shen, X. Tian and L. Zhang, *Mater. Chem. Phys.*, 2011, **131**, 358; (*c*) C. Zhang, Y. Che, Z. Zhang, X. Yang and L. Zang, *Chem. Commun.*, 2011, **47**, 2336; (*d*) Y. P. Wang, F. Wang, D. F. Luo, L. Zhou and L. L. Wen, *Inorg. Chem. Commun.*, 2012, **19**, 43; (*e*) A. Swarnkar, G. S. Shanker and A. Nag, *Chem. Commun.*, 2014, **50**, 4743.

9 (*a*) Y. N. Gong, L. Jiang and T. B. Lu, *Chem. Commun.*, 2013, **49**, 11113; (*b*) T. K. Kim, J. H. Lee, D. Moon and H. R. Moon, *Inorg. Chem.*, 2013, **52**, 589; (*c*) D. Ma, B. Li, X. Zhou, Q. Zhou, K. Liu, G. Zeng, G. Li, Z. Shi and S. Feng, *Chem. Commun.*, 2013, **49**, 8964; (*d*) Y. S. Xue, Y. He, L. Zhou, F. J. Chen, Y. Xu, H. B. Du, X. Z. You and B. Chen, *J. Mater. Chem. A.*, 2013, **1**, 4525; (*e*) S. Zhang, L. Han, L. Li, J. Cheng, D. Yuan and J. Luo, *Cryst. Growth Des.*, 2013, **13**, 5466; (*f*) X. Zhou, H. Li, H. Xiao, L. Li, Q. Zhao, T. Yang, J. Zuo and W. Huang, *Dalton Trans.*, 2013, **42**, 5718; (*g*) G. Y. Wang, C. Song, D. M. Kong, W. J. Ruan, Z. Chang and Y. Li, *J. Mater. Chem. A.*, 2014, **2**, 2213; (*h*) Y. Guo, X. Feng, T. Han, S. Wang, Z. Lin, Y. Dong and B. Wang, *J. Am. Chem. Soc.*, 2014, **136**, 15485.

10 (*a*) A. Lan, K. Li, H. Wu, D. H. Olson, T. J. Emge, W. Ki, M. Hong and J. Li, *Angew. Chem., Int. Ed.*, 2009, **48**, 2334; (*b*) S. Pramanik, C. Zheng, X. Zhang, T. J. Emge and J. Li, *J. Am. Chem. Soc.*, 2011, **133**, 4153; (*c*) R. Li, Y. P. Yuan, L. G. Qiu, W. Zhang and J. F. Zhu, *Small*, 2012, **8**, 225; (*d*) D. Banerjee, Z. Hu, S. Pramanik, X. Zhang, H. Wang and J. Li, *CrystEngComm*, 2013, **15**, 9745; (*e*) A. K. Chaudhari, S. S. Nagarkar, B. Joarder and S. K. Ghosh, *Cryst. Growth Des.*, 2013, **13**, 3716; (*f*) S. Pramanik, Z. Hu, X. Zhang, C. Zheng, S. Kelly and J. Li, *Chem.-Eur. J.*, 2013, **19**, 15964; (*g*) X. G. Liu, H. Wang, B. Chen, Y. Zou, Z. G. Gu, Z. Zhao and L. Shen, *Chem. Commun.*, 2014, **DOI:** 10.1039/C4CC08945F.

11 (*a*) S. S. Nagarkar, B. Joarder, A. K. Chaudhari, S. Mukherjee and S. K. Ghosh, *Angew. Chem., Int. Ed.*, 2013, **52**, 2881; (*b*) B. Joarder, A. V. Desai, P. Samanta, S. Mukherjee and S. K. Ghosh, *Chem.-Eur. J.*, 2014, **DOI:** 10.1002/chem.201405167; (*c*) S. S. Nagarkar, A. V. Desai and S. K. Ghosh, *Chem. Commun.*, 2014, **50**, 8915.

12 (*a*) E. R. Cooper, C. D. Andrews, P. S. Wheatley, P. B. Webb, P. Wormald and R. E. Morris, *Nature*, 2004, **430**, 1012; (*b*) E. R. Parnham and R. E. Morris, *J. Am. Chem. Soc.*, 2006, **128**, 2204; (*c*) E. R. Parnham, P. S. Wheatley and R. E. Morris, *Chem. Commun.*, 2006, 380; (*d*) B. T. Yonemoto, Z. Linb and F. Jiao, *Chem. Commun.*, 2012, **48**, 9132; (*e*) Y. Wei, B. Marler, L. Zhang, Z. Tian, H. Graetscha and H. Gies, *Dalton Trans.*, 2012, **41**, 12408.

13 (*a*) K. Jin, X. Y. Huang, L. Pang, J. Li, A. Appel and S. Wherland, *Chem. Commun.*, 2002, 2872; (*b*) D. N. Dybtsev, H. Chun and K. Kim, *Chem. Commun.*, 2004, 1594; (*c*) Z. J. Lin, A. M. Z. Slawin and R. E. Morris, *J. Am. Chem. Soc.*, 2007, **129**, 4880; (*d*) Z. J. Lin, D. S. Wragg, J. E. Warren and R. E. Morris, *J. Am. Chem. Soc.*, 2007, **129**, 10334; (*e*) J. Zhang, S. M. Chen and X. H. Bu, *Angew. Chem., Int. Ed.*, 2008, **47**, 5434.

14 (*a*) L. Xu, S. H. Yan, E. Y. Choi, J. Y. Lee and Y. U. Kwon, *Chem. Commun.*, 2009, 3431; (*b*) H. Ren, T. Ben, E. Wang, X. F. Jing, M. Xue, B. B. Liu, Y. Cui, S. L. Qiu and G. S. Zhu, *Chem. Commun.*, 2010, **46**, 291; (*c*) W. X. Chen, H. R. Xu, G. L. Zhuang, L. S. Long, R. B. Huang and L. S. Zheng, *Chem. Commun.*, 2011, **47**, 11933; (*d*) Y. Kang, S. M. Chen, F. Wang, J. Zhang and X. H. Bu, *Chem. Commun.*, 2011, **47**, 4950;

15 (*a*) W. M. Reichert, J. D. Holbrey, K. B. Vigour, T. D. Morgan, G. A. Broker and R. D. Rogers, *Chem. Commun.*, 2006, 4767; (*b*) Z. Fei, T. J. Geldbach, D. Zhao and P. J. Dyson, *Chem.-Eur. J.*, 2006, **12**, 2122; (*c*) E. R. Parnham and R. E. Morris, *Acc. Chem. Res.* 2007**, 40**, 1005; (*d*) R. E. Morris, *Chem. Commun.*, 2009, 2990; (*e*) E. Ahmed and M. Ruck, *Dalton Trans.*, 2011, **40**, 9347; (*f*) D. Freudenmann, S. Wolf, M. Wolff and C. Feldmann, *Angew. Chem., Int. Ed.*, 2011, **50**, 11050; (*g*) C. P. Li and M. Du, *Chem. Commun.*, 2011, 5958.

16 (*a*) D. Y. Du, J. S. Qin, C. X. Sun, X. L. Wang, S. R. Zhang, P. Shen, S. L. Li, Z. M. Su and Y. Q. Lan, *J. Mater. Chem.*, 2012, **22**, 19673. (*b*) J. Qin, Y. Jia, H. Li, B. Zhao, D. Wu, S. Zang, H. Hou and Y. Fan, *Inorg. Chem.*, 2014, **53**, 685.

17 *SMART and SAINT. Area Detector Control and Integration Software*; Siemens Analytical X-Ray Systems, Inc.: Madison, WI, 1996.

18 Sheldrick, G. M. *SHELXS-97: Program for the Solution of Crystal Structure*; University of Göttingen: Göttingen, Germany, 1997.

19 Sheldrick, G. M. *SHELXL-97, Program for the Crystal Structure Refinement*; University of Göttingen: Göttingen, Germany, 1997.

20 Sheldrick, G. M. *SADABS Siemens Area Correction Absorption Program*; University of Göttingen: Göttingen, Germany, 1994.

21 Spek, A. L. *Implemented as the PLATON Procedure, a Multipurpose Crystallographic Tool*; Utrecht University: Utrecht, The Netherlands, 1998.

22 (*a*) M. Eddaoudi, D. B. Moler, H. Li, B. Chen, T. M. Reineke, M. O'Keeffe and O. M. Yaghi, *Acc. Chem. Res.*, 2001, **34**, 319; (*b*) O. M. Yaghi, M. O'Keeffe, N. W. Ockwig, H. K. Chae, M. Eddaoudi and J. Kim, *Nature*, 2003, **423**, 705; (*c*) T. Kajiwara, K. Katagiri, M. Hasegawa, A. Ishii, M. Ferbinteanu, S.Takaishi, T. Ito, M. Yamashita and N. Iki, *Inorg. Chem.*, 2006, **45**, 4880; (*d*) D. Savard, P. H. Lin, T. J. Burchell, I. Korobkov, W. Wernsdorfer, R. Clérac and M. Murugesu, *Inorg. Chem.*, 2009, **48**, 11748; (*e*) J. B. Peng, Y. P. Ren, X. J. Kong, L. S. Long, R. B. Huang and L. S. Zheng, *CrystEngComm*, 2011, **13**, 2084; (*f*) J. M. Zhou, W. Shi, H. M. Li, H. Li and P. Cheng, *J. Phys. Chem. C.*, 2014, **118**, 416.

23 (*a*) S. M. Aly, M. R. Parida, E. Alarousu and O. F. Mohammed, *Chem. Commun.*, 2014, **50**, 10452; (*b*) A. O. El-Balouli, E. Alarousu, M. Bernardi, S.t M. Aly, A. P. Lagrow, O. M. Bakr and O. F. Mohammed, *J. Am. Chem. Soc.*, 2014, **136**, 6952; (*c*) S. M. Aly, S. Goswami, Q. A. Alsulami, K. S. Schanze and O. F. Mohammed, *J. Phys. Chem. Lett.*, 2014, **5**, 3386; (*d*) O. F. Mohammed, D. Masih, S. M. Aly and E. Alarousu, *J. Mater. Chem. A.*, 2015, **DOI:** 10.1039/C4TA07033J.

24 (*a*) B. Gole, A. K. Bar and P. S. Mukherjee, *Chem.-Eur. J.*, 2014, **20**, 2276; (*b*) D. Tian, Y. Li, R. Y. Chen, Z. Chang, G. Y. Wang and X. H. Bu, *J. Mater. Chem. A.*, 2014, **2**, 1465; (*c*) Q. Zhang, A. Geng, H. Zhang, F. Hu, Z. H. Lu, D. Sun, X. Wei and C. Ma, *Chem.-Eur. J.*, 2014, **20**, 4885; (*d*) S. R. Zhang, D. Y. Du, J. S. Qin, S. J. Bao, S. L. Li, W. W. He, Y. Q. Lan, P. Shen and Z. M. Su, *Chem.-Eur. J.*, 2014, **20**, 3589; (*e*) D. Tian, R. Y, Chen, J. Xu, Y. W. Li and X. H. Bu, *APL Mat.*, 2014, **2**, 124111; (*f*) Q. Chen, Z. Chang, W. C. Song, H. Song, H. B. Song, T. L. Hu and X. H. Bu, *Angew. Chem., Int. Ed.*, 2013, **52**, 11550.

25 (*a*) L. Sun, H. Xing, J. Xu, Z. Liang, J. Yu and R. Xu, *Dalton Trans.*, 2013, **42**, 5508; (*b*) J. Ye, L. Zhao, R. F. Bogale, Y. Gao, X. Wang, X. Qian, S. Guo, J. Zhao and G. Ning, *Chem.-Eur. J.*, 2014, **DOI:** 10.1002/chem.201405267.

Aqueous- and vapor-phase detection of nitroaromatic explosives by a water-stable fluorescent microporous MOF directed by ionic liquid

Jianhua Qin,[a,b] Bing Ma,[a] Xiao-Fei Liu,[a] Hong-Lin Lu,[a] Xi-Yan Dong,[a] Shuang-Quan Zang*[a] and Hongwei Hou*[a]

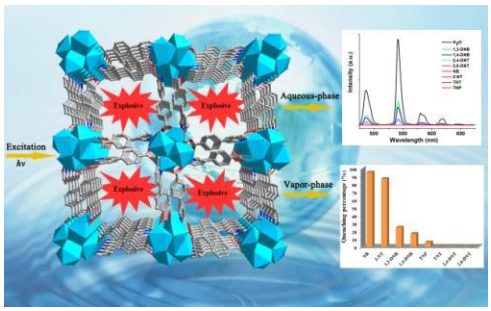

Aqueous- and vapor-phase detection of nitroaromatic explosives by a water-stable fluorescent microporous MOF directed by ionic liquid.